Journal of Crystal Growth 132 (1993) 250–260
North-Holland

JOURNAL OF CRYSTAL GROWTH

Characterization of precipitates in CdTe and $Cd_{1-x}Zn_xTe$ grown by vertical Bridgman–Stockbarger technique

J. Shen, D.K. Aidun, L. Regel and W.R. Wilcox

Consortium for Commercial Crystal Growth, Clarkson University, Potsdam, New York 13699, USA

Received 10 March 1993; manuscript received in final form 10 May 1993

Different polishing solutions were tested for exposing precipitates in CdTe and $Cd_{0.96}Zn_{0.04}$ single crystals grown by vertical Bridgman–Stockbarger technique. A solution of 5–7% Br_2 in methanol and E-solution were both effective. High resolution scanning electron microscopy with energy dispersive spectroscopy (SEM/EDS) was employed to characterize those exposed precipitates. Most of the polyhedral-shaped Te precipitates with a size range from 3 to 20 μm had voids inside. Partially dissolved Te precipitates were observed in CdTe samples that had been annealed in Cd vapor at 700°C for 10 min. Isolated areas mis-oriented from the matrix were observed in CdTe and $Cd_{0.96}Zn_{0.04}Te$ that had been annealed in Cd vapor at 700°C for 20 and 50 h, respectively. Te precipitate images were recorded with EDS. By SEM/EDS, Cd-rich precipitates were observed in some Cd-annealed CdTe. C and Na impurities were detected in some Te precipitates.

1. Introduction

Precipitates are common defects in CdTe and Zn-doped CdTe crystals [1,2]. Those precipitates are detrimental to the quality of CdTe and to HgCdTe epitaxial layers grown on CdTe or CdZnTe substrates [1]. Large Te precipitates with a dimension of about 3–20 μm are often observed in CdTe and CdZnTe ingots grown by the vertical Bridgman–Stockbarger (VBS) technique [2,3]. Post-growth annealing in Cd vapor is often performed to diminish those precipitates. It is believed that precipitates form during growth and post-growth cooling as a consequence of non-stoichiometric melts and the retrograde solid solubilities of Cd and Te in CdTe [4,5].

Few reports on the morphology of precipitates in CdTe are in the literature [2,6]. Further, it is difficult to accurately identify precipitate compositions. Precisely characterizing precipitates would be helpful to further understand the origin of precipitates during VBS-growth and to improve the post-growth annealing process.

Precipitates larger than about 1 μm in bulk CdTe can be observed by infrared microscopy (IRM) and cathodoluminescence scanning electron microscopy (SEM-CL) [2,4,7–8]. However, those techniques cannot give the morphological detail of a precipitate. Only a blurry image can be seen under IRM and SEM-CL. For precipitates smaller than about 1 μm, transmission electron microscopy (TEM) has been applied [9–11].

To identify the composition and structure of precipitates, X-ray diffraction (XRD) [6,12], Auger electron spectroscopy (AES) [2,6], TEM with energy dispersive spectroscopy (TEM/EDS) [7,9] and TEM electron diffraction (TEM/ED) [13] have been employed. Most of the above techniques for composition identification are effective only near the very shallow surface layer. XRD and TEM/ED methods usually did not generate much information, because of low precipitate density, small precipitate size, and the weak Te peaks that were mixed with background noise or peaks from other phases [13–14]. Most of the above techniques require a very flat sample. Further, it is difficult to observe the precipitate morphology using TEM, because CdTe is fragile and the precipitate size (1–20 μm) in as-grown CdTe normally is larger than the TEM

sample's thickness (about 1000 Å) [13]. Therefore, to properly characterize precipitates in CdTe with the above techniques, sample preparation is critical. Polishing solutions often used for characterizing precipitates are summarized in table 1. As seen in the table, Br_2 in methanol was the most used one.

In the present study, various etching methods were tested for exposing precipitates in CdTe and $Cd_{0.96}Zn_{0.04}Te$. IR microscopy and high resolution SEM/EDS were used to characterize the precipitates. We developed a procedure for characterizing precipitates without destroying their original morphology. Based on the characterization results, a mechanism for the formation of large precipitates during VBS growth is suggested.

2. Experiments

The CdTe ingots used in these experiments were grown in our laboratory by the vertical Bridgman-Stockbarger (VBS) technique. The starting material for CdTe growth was obtained from II-VI Inc. $Cd_{0.96}Zn_{0.04}Te$ wafers were cut from an ingot grown at II-VI Inc. by a modified VBS technique. The original purities of the starting materials were reported to be all 6 N. The growth furnace in our laboratory was a two-zone VBS furnace with the following growth parameters: translation rate, 2 mm/h; furnace temperature gradient near the solid–melt interface, about 2.5°C/cm; hot zone and cold zone temperatures, 1120 and 1080°C, respectively; post-growth cooling rate: 10°C/h from 1090 to 1000°C, 20°C/h from 1000 to 800°C and 50°C/h below 800°C. The quartz ampoules for growth were coated with a thin film of carbon.

CdTe and $Cd_{0.96}Zn_{0.04}Te$ single crystal wafers with a thickness of 2.0 mm were mined from ingots and sectioned into 15×20 mm^2 pieces. All wafers were oriented into {111} planes by Laue method. Some of the wafers were annealed in saturated Cd or Te vapor at 700°C in well cleaned and evacuated ($< 10^{-6}$ Torr) quartz ampoules. The annealing time was varied between 10 min and 50 h. Both sides of the wafers were mechanically polished, and then chemically polished in 2% Br–methanol before annealing. The cooling rate after annealing was 33°C/h from 700 to 500°C, and then the power was shut off.

To prepare the wafers for IR microscopy, both sides were repolished as before annealing. Finally, wafers about 1.5 mm thick were cleaned in de-ionized water and dried in air. The sample preparation for SEM/EDS analysis will be detailed in the next section.

3. Results and discussion

3.1. Chemical polishing for exposing precipitates

In addition to polishing CdTe and $Cd_{0.96}Zn_{0.04}Te$ samples, Cd shot and Te chunks were etched by the solutions listed in table 1. It was found that Br_2 in methanol (BM) gave the lowest etching rates of all these solutions. For instance, Cd was removed in 2% BM at about 2.25 μm/min and Te 1.25 μm/min. On the other hand, a CdTe wafer was thinned in 2% BM at about 7.5 μm/min (all etching rates are on one side of a sample). Thus, the etching rates of Cd or Te

Table 1
Chemical polishing solutions for CdTe and CdZnTe

No.	Chemical polishing solution	Characterization technique	Reference
1	$K_2Cr_2O_7 + HNO_3 + H_2O$	TEM/ED	[13]
2	Br_2 + methanol (Br_2 % unspecified)	AES, SEM-CL, XRD, TEM/EDS	[4,6,9]
3	$H_2SO_4 + K_2Cr_2O_7 + H_2O$	SEM, AES	[19]
4	2% Br_2 + methanol	TEM/EDS	[10,15]
5	5% Br_2 + methanol (Ar ion beam etching)	AES, IRM	[2]

precipitates in low concentration BM solution are less than CdTe. In addition, E-solution (10 ml HNO_3 + 20 ml H_2O + 4g $K_2Cr_2O_7$) gave the second lowest etching rate for Te. Based on the above tests, Br_2–methanol with a Br_2 concentration from 1% to 10% and E-solution were selected as the solutions to be tested for exposing precipitates in CdTe.

By extensive polishing tests with all the above-mentioned solutions and careful observation under the optical microscope and SEM, the following procedure was proven to be effective for exposing precipitates on (111)-oriented CdTe and $Cd_{0.96}Zn_{0.04}Te$ surfaces:

(1) Mechanically polish with 0.3–5.0 μm alumina particles followed by 2% BM for 3 min.

(2) Ultrasonically clean in acetone.

(3) 5%–7% BM for 2 min or E-solution for 40s followed by a rinse in de-ionized water.

The results from the above procedure are illustrated in figs. 1 and 2. With SEM/EDS, the exposed second phases in figs. 1 and 2 were proven to be Te precipitates, as seen in figs. 7 and 8.

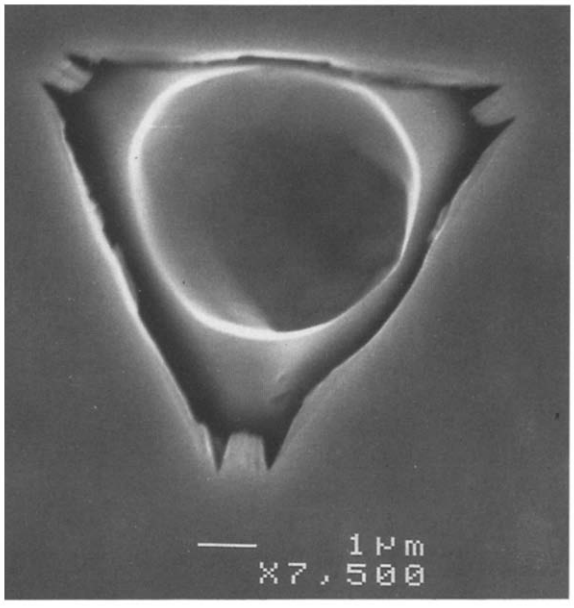

Fig. 2. SEM micrograph showing a void in a precipitate in as-grown CdTe. The precipitate was exposed on (111)A by E-solution.

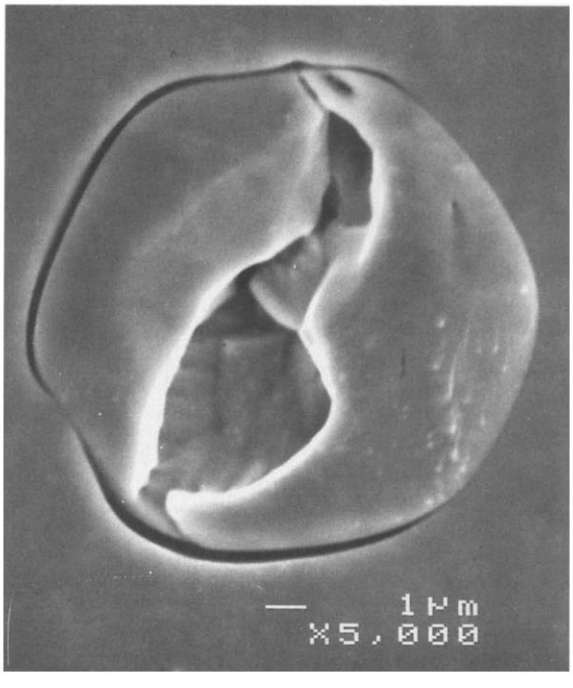

Fig. 1. SEM micrograph showing a cavity in a precipitate in as-grown CdTe. The precipitate was exposed on (111)A by 6% Br_2–methanol.

As shown in figs. 1 and 2, Te precipitates exposed by Br_2 in methanol formed plateaus, while those exposed by E-solution lay in valley-shaped triangular etch pits. Considering the etch rate difference between Te and CdTe mentioned above, the former might have caused by the faster etching rate of CdTe than of Te precipitates in Br_2-methanol. For the latter, it may mean that the E-solution is more sensitive to the heavy strained material around a precipitate than is Br_2 in methanol. Under TEM it was seen that dislocations [9] and the radial strain fields [15] surround precipitates. According to our observation, star-shaped features consisting of piled-up etch pits were often observed on a (111)A plane etched with Nakagawa solution. Those star features were believed to have originated from dislocations formed by prismatic punch deformation around large precipitates [2]. Therefore, E-solution could have attacked the strained CdTe matrix around precipitates more rapidly than etched away the rest of the CdTe surface.

In addition to the solutions mentioned above, we also tried many other solutions reported in the literature. Generally it was found that solutions containing H_2SO_4, H_2O_2 or HF could not clearly expose precipitates on CdTe surfaces. This was not surprising, because those chemicals are main components in most of the solutions recommended for etching or polishing elemental Te [16]. Comparing to E-solution, Br_2–methanol seemed to be less-destructive to precipitates. Thus, it was possible to observe the original morphology of precipitates using optical microscopy or SEM.

3.2. Precipitate morphology

As seen in fig. 3, under IR transmission microscopy, needle cluster and cloud-shaped precipitates were observed in some CdTe and $Cd_{0.96}Zn_{0.04}Te$ samples that were either as-grown or annealed in Cd vapor. Those precipitates were smaller than 1 μm. The needles and the clouds all were roughly ⟨211⟩-oriented on {111} planes. The {111}⟨211⟩ are the usual directions along which dislocations and stacking faults lie [9,17]. Therefore, it is reasonable to attribute the formation of those precipitates to the deposition of excessive Te along dislocations and stacking faults during growth and cooling. Those precipitates were not seen on surfaces by either polishing solution. Commonly, irregular tiny pits or valleys could be observed on the surfaces of the above samples. In the areas with clusters of small precipitates, the densities of dislocations and stacking faults could be very high. The lattice strain in these areas might have be severe. Thus, those small precipitates could have wholly removed with their surrounding matrix during etching with either solution.

As illustrated in fig. 4, under IR microscopy from the ⟨111⟩ direction, precipitates larger than 1 μm appeared as either triangles with curved sides or as hexagons with edges parallel or normal to ⟨110⟩ directions, respectively. As shown in

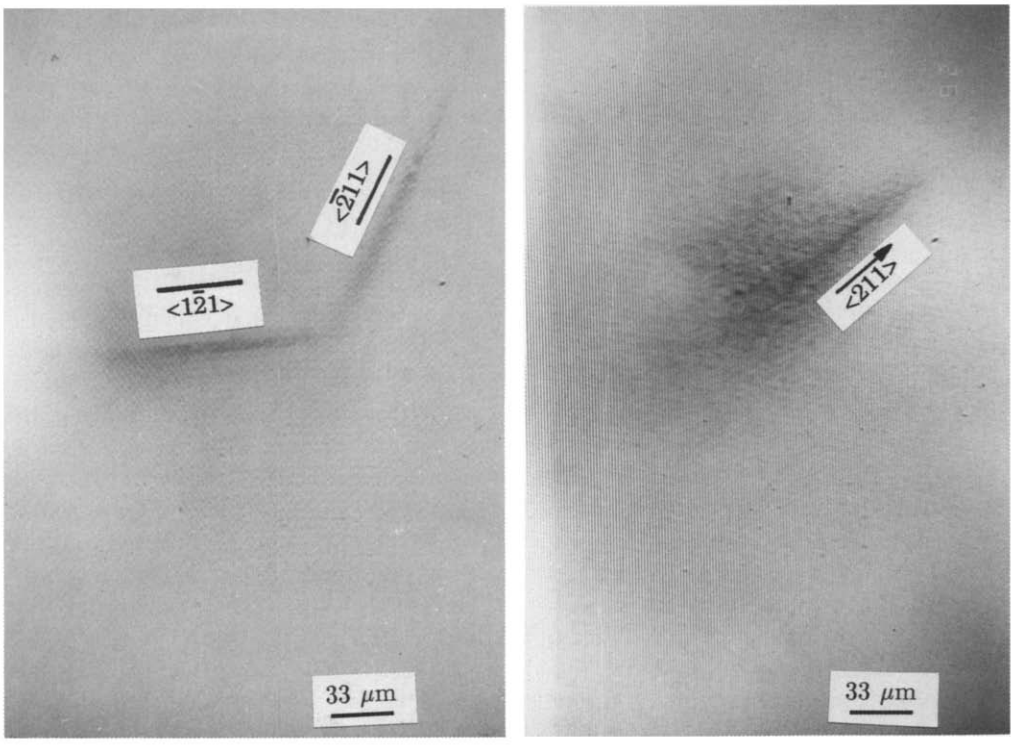

Fig. 3. Needle cluster and cloud-shaped precipitate in $Cd_{0.96}Zn_{0.04}Te$ under IR microscope. Observed from ⟨111⟩.

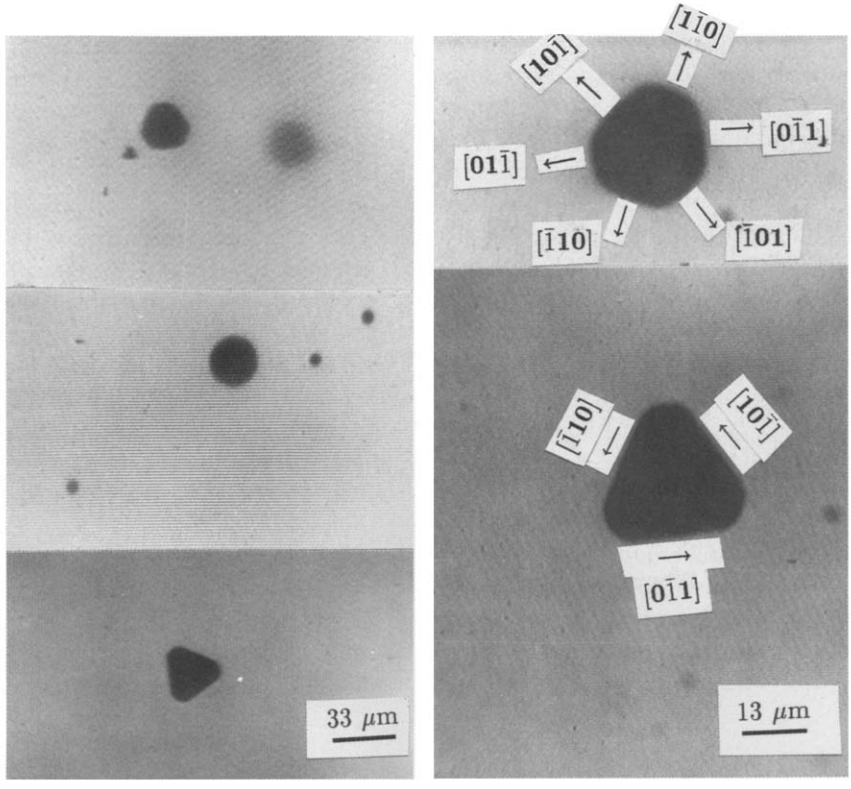

Fig. 4. Morphology of large precipitates in $Cd_{0.96}Zn_{0.04}Te$ under IR microscope. Observed from ⟨111⟩.

figs. 1 and 2, precipitates exposed on {111} surfaces appeared to be either triangular or hexagonal. Note that the intersection of a (111) plane with a {110} polygon is either a triangle or a hexagon. Therefore, it is likely that the precipitates were polyhedral with {110} facets.

No large precipitates were seen on the wafers annealed in Cd for longer than 30 minutes; Te precipitates may have been dissolved into smaller ones or converted to CdTe.

As illustrated in the scanning electron micrograph of fig. 1, cavities deeply penetrated into most of the precipitates larger than 5 μm. Irregularly-shaped voids were in most of the precipitates between 3 to 5 μm, as seen in fig. 2. Most of these voids were inside precipitates, rather than at precipitate edges, as seen in figs. 1 and 2. Precipitates without voids inside were occasionally observed. A high fraction of the large precipitates had voids in the as-grown CdTe and $Cd_{0.96}Zn_{0.04}Te$.

We suggest a formation mechanism for the large precipitates during VBS growth. Some tiny gas bubbles might have been dissolved into CdTe melt. The bubbles could be H_2 and Ar. The former might decompose at elevated temperatures from the residual water vapor that existed in the starting materials and the ampoule. The latter might be induced by the backfilling of Ar during ampoule evacuation. During solidification, those dissolved tiny gas bubbles could be rejected from solidified CdTe, and accumulate near the freezing interface. Then, relatively large gas bubbles could form and be trapped at the interface. During cooling, excessive Te or Cd atoms and impurities might have deposited near those bubbles as a consequence of retrograde solid solubilities of Te or Cd. Thus, precipitates with voids

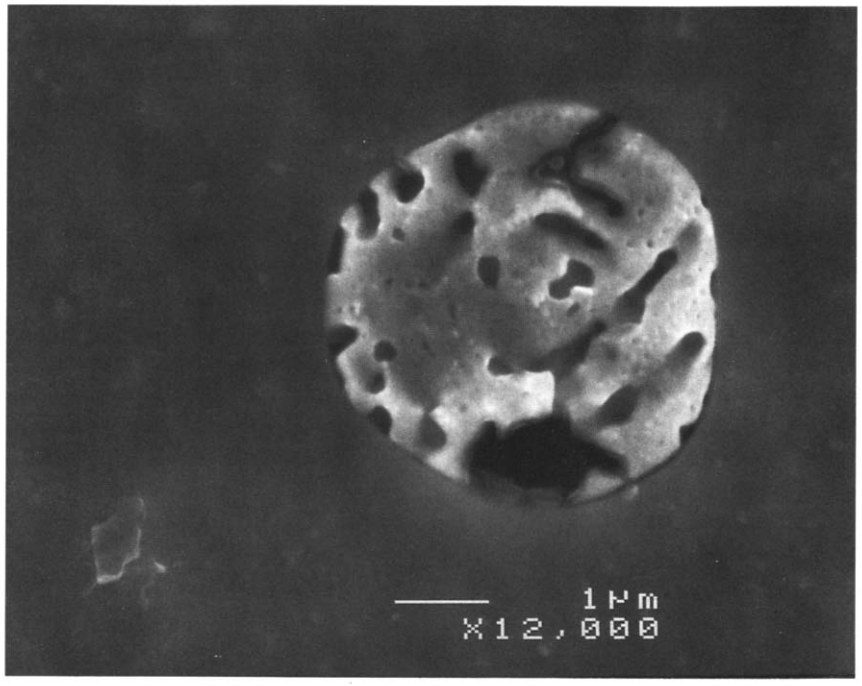

Fig. 5. A precipitate in CdTe annealed in Cd vapor at 700°C for 10 min. The precipitate was exposed on (111)A by 5%Br_2–methanol.

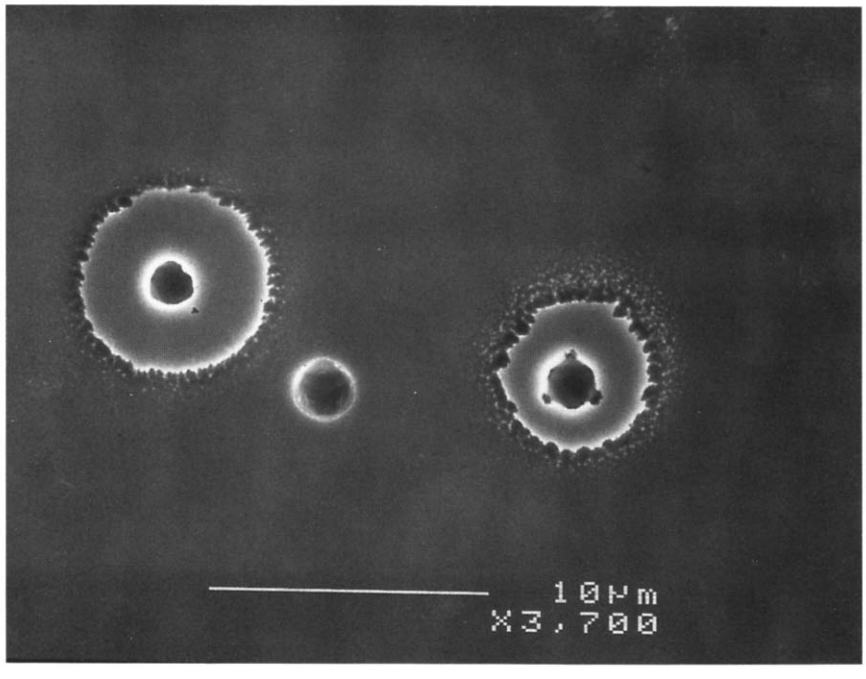

Fig. 6. Isolated areas in CdTe matrix. The sample was annealed in Cd vapor at 700°C for 20 h. The (111)A surface was polished by E-solution.

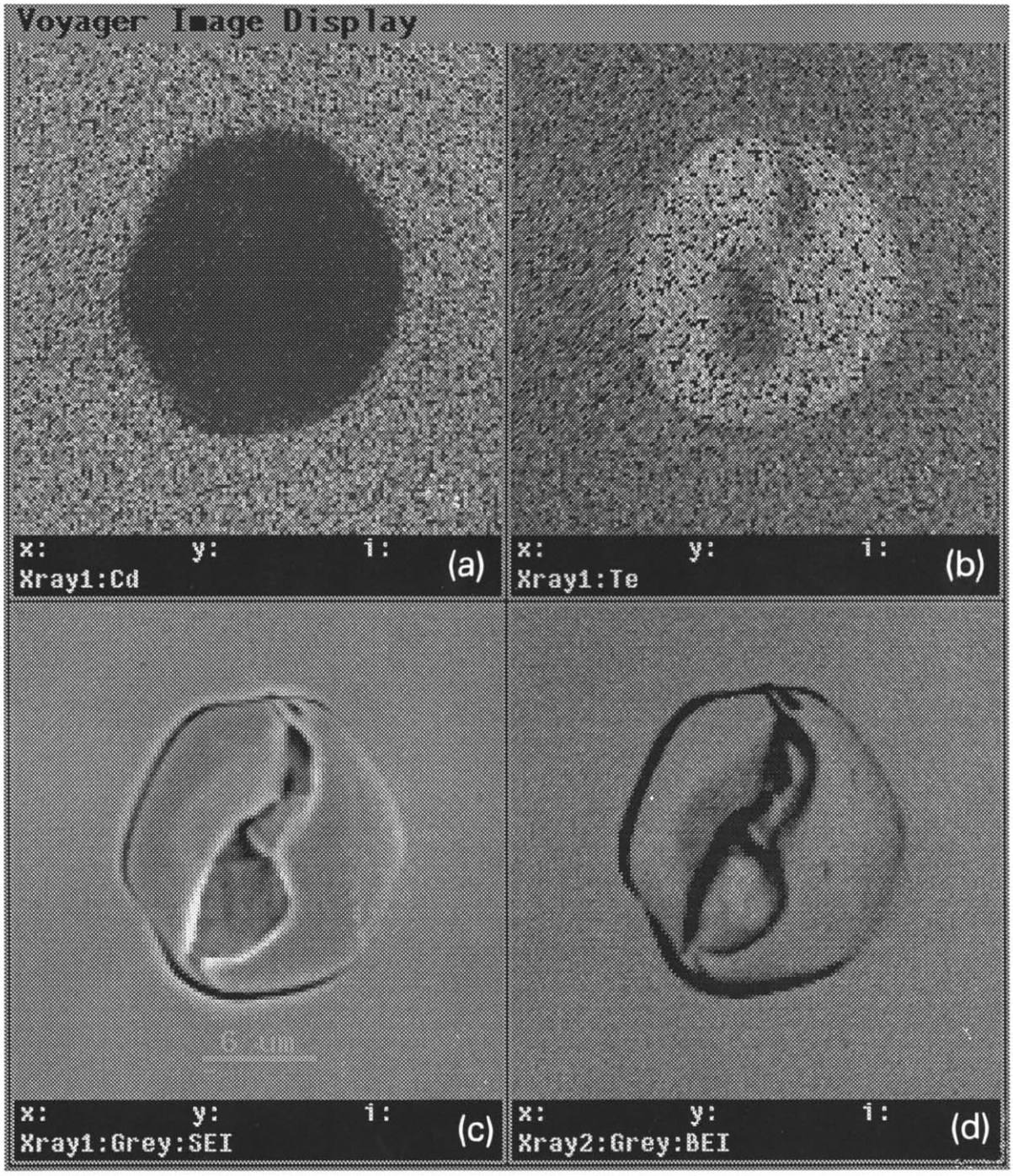

Fig. 7. SEM/EDS images of the precipitate shown in fig. 1. (a) X-ray energy for elemental Cd. The dark area shows an absence of Cd. (b) X-ray energy for elemental Te. The bright area shows presence of Te. (c) SEM/SEI mode. The contrast shows surface roughness. (d) SEM/BEI mode. The contrast is sensitive to surface flatness, but not to the composition difference between CdTe and Te.

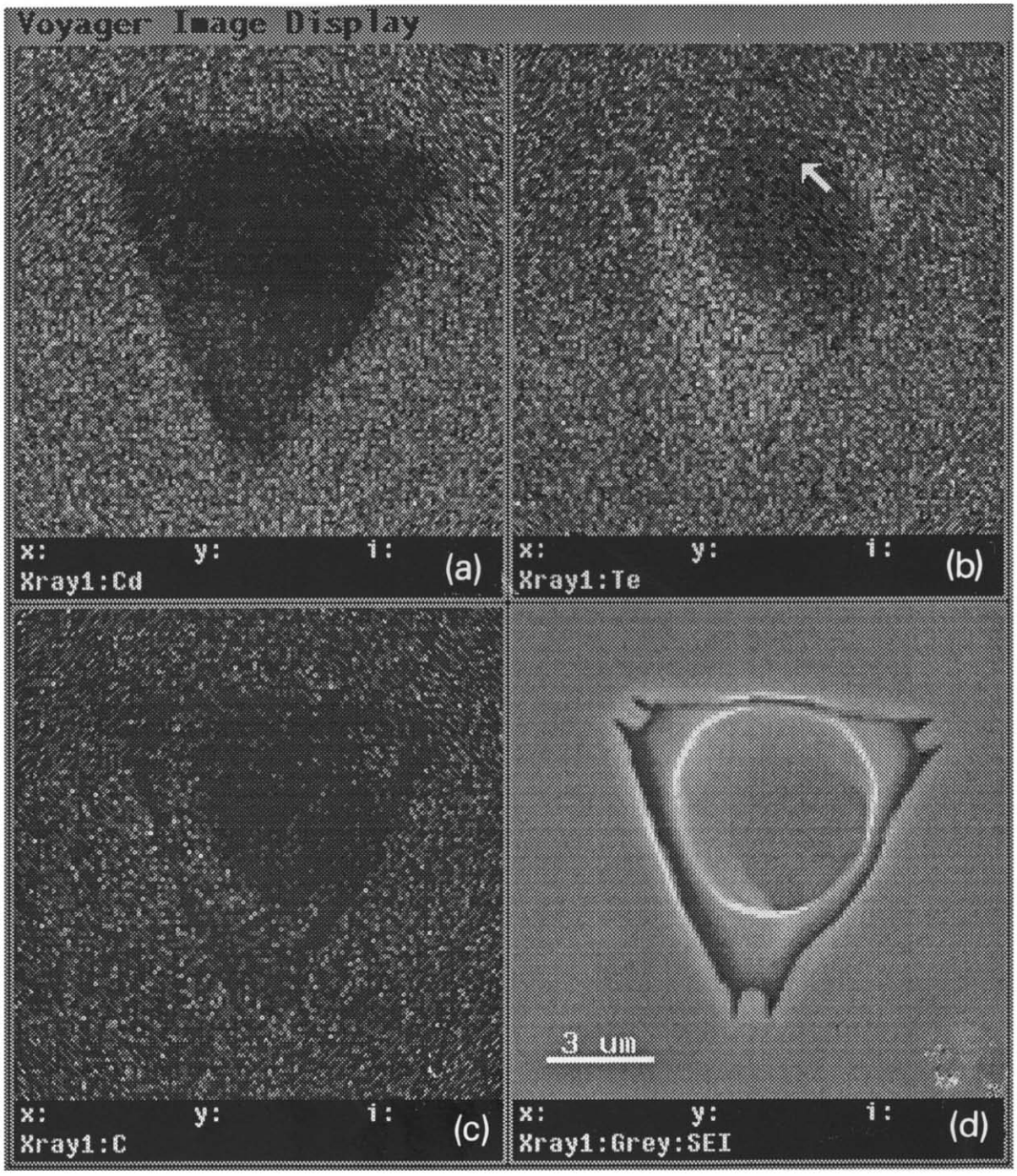

Fig. 8. SEM/EDS images of the precipitate shown in fig. 2. (a) X-ray energy for elemental Cd. (b) X-ray energy for elemental Te. (c) X-ray energy for elemental C. No detectable C was formed around the precipitate. (d) SEM/SEI mode of the precipitate.

would form in the as-grown CdTe. On the other hand, if the starting CdTe melt was Te- or Cd-rich, Te- or Cd-rich droplets might have been associated with the accumulated gas bubbles, and trapped at the interface as a result of constitutional supercooling. Thus, precipitates with voids would directly form during growth.

As seen in the next section, with EDS measurement, C and Na were detected around or in some of the precipitates. In some precipitates, no detectable amount of impurities were found in and around the cavities. In addition, bubbles were often observed near the centers or on the surfaces of CdTe ingots grown by the VBS technique.

As shown in fig. 5, Te precipitates between 1 and 3 μm with many voids were often observed on CdTe samples which had been annealed in Cd vapor at 700°C for 10 min. Cd peaks were detected in and around these voids by EDS. These exposed precipitates were observed after the wafer had been polished to a depth of 210 μm.

No large precipitates could be observed in the CdTe samples annealed in Cd vapor at 700°C for 20 or 50 h. However, some isolated circular areas with a size from 5 to 125 μm were frequently observed on surfaces etched by E-solution, as seen in fig. 6. Those areas were oriented differently from the original CdTe matrix. EDS showed that some of those areas were CdTe and some were Cd-rich CdTe. We suggest that this could have been caused by the conversion of the existing Te precipitates to CdTe by the in-diffusing Cd atoms. Further, annealing in Cd vapor for a long time (20 or 50 h), excess Cd atoms might have deposited around the Te droplets and formed Cd-rich CdTe.

In samples annealed in saturated Te vapor at 700°C for 20 h, no isolated areas could be observed. Large irregularly-shaped Te precipitates were observed.

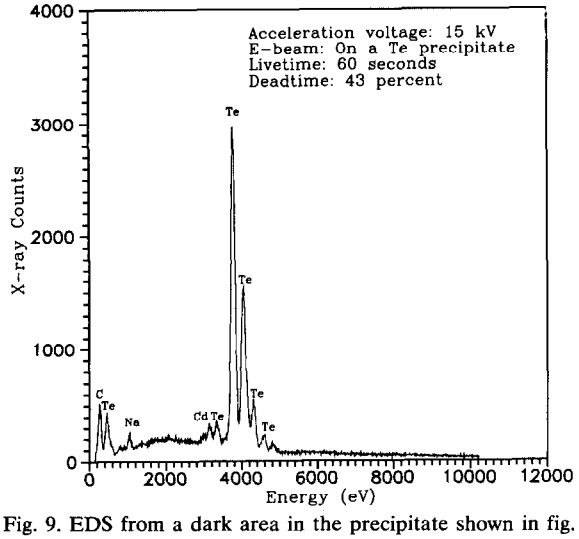

Fig. 9. EDS from a dark area in the precipitate shown in fig. 5. In addition to strong Te peaks, peaks from C and Na were observed.

3.3. Precipitate composition

The contrast in a SEM back-scattering electron image (BEI) is sensitive to both surface flatness and the atomic number Z of the sample. The contrast in a SEM secondary electron image (SEI) is sensitive only to the surface flatness and the extra electron charge accumulating on the surface from the SEM primary electron beam [18]. Therefore, a composition difference would be observed in the SEM/BEI mode only if the sample surface is flat and the atomic numbers are not very close. As seen in the lower right-hand corner image in fig. 7, for a Te precipitate on a CdTe surface, the SEM/BEI contrast was not sufficient to tell a composition difference. Only the shadow caused by the cavity could be seen. This was caused by the fact that the average atomic number for CdTe (50) is close both to that of Cd (48) and Te (52). As a solution to the above problem, EDS was employed to display the composition of precipitates exposed on CdTe surfaces. This method has the advantages of high sensitivity (0.1% to 1%) for Cd and Te, high resolution of incident beam (about 50 to 100 Å) [18], and a readily observable image. The characteristic X-ray "L lines" from Cd and Te were selected to image the precipitate area. Figs. 7 and 8 are two examples of EDS images, which correspond to the areas of the scanning electron micrographs in figs. 1 and 2. The bright area shows the presence of the characteristic X-rays from Te. Normally, it requires strong X-ray signal to pro-

duce an image. Thus, all of the above images showed that those precipitates mainly consisted of elemental Te. The result was confirmed by energy dispersive spectrum.

As seen in the above EDS images, X-ray signals from elemental C and Cd were not sufficient to produce bright EDS images. However, weak peaks from C and Na showed in EDS of the same precipitates, as seen in fig. 9. This means that the amount of C and Na in the precipitate was above 10^{19}–10^{20} atoms/cm^3 which generally is the detection limit of EDS [18]. In addition to C and Na, elemental K, O, Cl and S were also detected in precipitates by the AES technique [4].

It was reported that most of the above impurities in CdTe have a segregation coefficient less than 1 [4,5]. Hence, those impurities would have accumulated in captured melt droplets during growth and post-growth in-situ annealing. When precipitates are dissolved by annealing in Cd vapor, those impurities could be released into the CdTe matrix and degrade the CdTe quality. In some of our Cd-annealing experiments, the IR transmission and electric properties of CdTe were worse than in as-grown CdTe. The release of impurities from precipitates might have been partly responsible. In this sense, efforts to minimize the density and size of captured melt during growth may also be beneficial in reducing impurities in annealed CdTe.

4. Summary

Proper etching can be very useful in characterizing precipitates in CdTe. We showed that 5–7% Br_2–methanol and E-solution are effective in exposing precipitates in CdTe and $Cd_{0.96}Zn_{0.04}Te$. High resolution SEM/EDS was employed to characterize the exposed precipitates.

Under SEM, most of the polyhedral-shaped Te precipitates with a size from 3 to 20 μm had voids inside. These precipitates may have formed by capturing melt and bubbles at the solid–liquid interface during solidification. Partially dissolved Te precipitates were observed in CdTe samples annealed in Cd vapor for 10 min. Isolated areas misoriented with the CdTe matrix were observed in CdTe and $Cd_{0.96}Zn_{0.04}Te$ samples annealed in Cd vapor for 20 and 50 h.

Precipitates smaller than 1 μm could not be observed on etched surfaces.

With EDS, Te precipitate images were recorded in CdTe and $Cd_{0.96}Zn_{0.04}Te$. Cd-rich precipitates were observed in some Cd-annealed CdTe. Impurities of C and Na were detected in some Te precipitates.

Acknowledgements

This work was supported by the Consortium for Commercial Crystal Growth, one of NASA's Centers for the Commercial Development of Space. The CdTe used for the experiments were provided by II-VI, Inc. in Saxonburg, PA. We are grateful to Mr. W. Plunkett for his help in SEM/EDS analyses.

References

[1] J.J. Kennedy, P.M. Amirtharaj, P.R. Boyd, S.B. Qadri, R.C. Dobbyn and G.G. Long, J. Crystal Growth 86 (1988) 93.
[2] M. Wada and J. Suzuki, Japan. J. Appl. Phys. 27 (1988) L972.
[3] H.R. Vydyanath, J. Ellsworth, J.J. Kennedy, B. Dean, C.J. Johnson, G.T. Neugebauer, J. Sepich and P. Liao, J. Vacuum Sci. Technol., in press.
[4] J.L. Pautrat, N. Magnea and J.P. Faurie, J. Appl. Phys. 53 (1982) 8668.
[5] K. Zanio, in: Semiconductors and Semimetals, Vol. 13, Cadmium Telluride (Academic Press, New York, 1978) pp. 124, 48.
[6] S.H. Shin, J. Bajaj, L.A. Moudy and D.T. Cheung, Appl. Phys. Letters 43 (1983) 68.
[7] S. McDevitt, B.E. Dean, D.G. Ryding, F.J. Scheltens and S. Mahajan, Mater. Letters 4 (1986) 451.
[8] Y.-C. Lu, R.S. Feigelson, R.K. Route and Z.U. Rek, J. Vacuum Sci. Technol. A 4 (1986) 2190.
[9] Y.Y. Loginov, P.D. Brown, N. Thompson, G.L. Russell and J. Woods, in: Microscopy of Semiconducting Materials 1989, Inst. Phys. Conf. Ser. 100, Eds. A.G. Cullis and J.L. Hutchison (Inst. Phys., Bristol, 1989) p. 433.
[10] A. Nouruzi-Khorasani and P.S. Dobson, J. Crystal Growth 92 (1988) 208.
[11] H.F. Schaake and J.H. Tregilgas, J. Electron. Mater. 12 (1983) 931.

[12] M. Takahashi, K. Uosaki, H. Kita and Y. Suzuki, J. Appl. Phys. 58 (1985) 4292.
[13] G.H. Narayanan and S.H. Rustomji, J. Electrochem. Soc. 126 (1979) 809.
[14] F.A. Selim, V. Swaminathan and F.A. Kröger, Phys. Status Solidi (a) 29 (1975) 465.
[15] K. Durose, G.J. Russell and J. Woods, J. Crystal Growth 72 (1985) 85.
[16] K. Sangwal, in: Defects in Solids, Vol. 15: Etching of Crystals, Eds. S. Amelinckx and J. Nihoul (North-Holland, Amsterdam, 1987) pp. 421–438.
[17] H.F. Schaake, J.H. Tregilgas, J.D. Beck, M.A. Kinch and B.E. Gnade, J. Vacuum Sci. Technol. A 3 (1985) 143.
[18] D.K. Schroder, in: Semiconductor Material and Device Characterization (Wiley, New York, 1990) pp. 507–538.
[19] K. Yokota, T. Yoshikawa, S. Katayama, S. Ishhara and I. Kimura, Japan. J. Appl. Phys. 24 (1985) 1672.